Catalysis with a Skip: Dynamically Coupled Addition, Proton Transfer, and Elimination During Au- and Pd-Catalyzed Diol Cyclization

Matthew S. Teynor, Windsor Scott, and Daniel H. Ess*

Department of Chemistry and Biochemistry, Brigham Young University, Provo, Utah 84602

Abstract

Au and Pd complexes have emerged as highly effective π-bond cyclization catalysts to construct heterocycles. These cyclization reactions are generally proposed to proceed through multi-step addition-elimination mechanisms involving Au- or Pd-alkyl intermediates. For Au- and Pd-catalyzed allylic diol cyclization, while the DFT potential energy surface landscapes show a stepwise sequence of alkoxylation π-addition, proton transfer, and water elimination, quasiclassical direct dynamics simulations reveal dynamical mechanisms that depend on the metal center. For Au, trajectories reveal that after π-addition the Au-alkyl intermediate is always skipped because addition is dynamically coupled with proton transfer and water elimination. In contrast, for Pd catalysis, due to differences in the potential-energy landscape shape, only about half of trajectories show Pd-alkyl intermediate skipping. The other half of the trajectories show the traditional two-step mechanism with the intervening Pd-alkyl intermediate. Overall, this work reveals that interpretation of a DFT potential-energy landscape can be insufficient to understand catalytic intermediates and mechanisms and that atomic momenta through dynamics simulations are needed to determine if an intermediate is genuinely part of a catalytic cycle.

Keywords

Gold, palladium, cyclization, density functional theory, molecular dynamics

Introduction

Molecular Au and Pd complexes have emerged as effective alkene cyclization catalysts to construct heterocycles.[1,2,3,4] These cyclization reactions are often proposed to proceed through multi-step mechanisms involving key Au- or Pd-alkyl intermediates.[5,6,7] Because protodemetalation of these metal-alkyl intermediates can be slow,[8] it was advantageous when Aponick[9,10,11,12] and Uenishi[13,14] independently reported Au-catalyzed and Pd-catalyzed cyclization of monoallyic diols that do not require protodemetalation. Scheme 1a shows that both Au and Pd catalyze cyclization and dehydration to give the vinyl tetrahydropyran product through an overall S_N2' transformation.

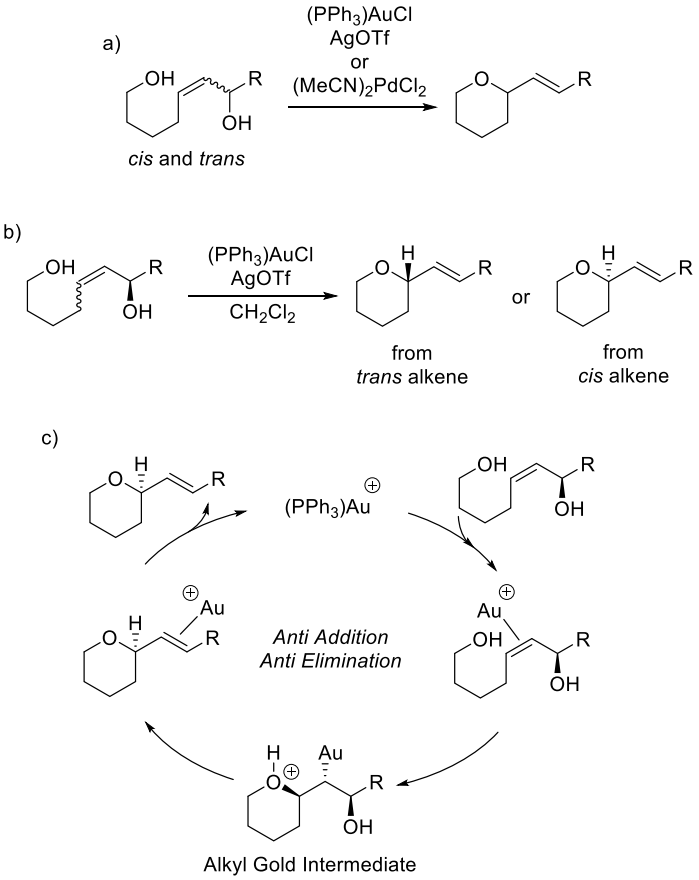

Scheme 1. a) General outline of Au- and Pd-catalyzed monoallyic diol cyclizations of *cis* and *trans* alkenes to tetrahydropyrans reported by Aponick[9] and Uenishi.[13] b) Example of chirality transfer for enantioenriched diols containing a chiral center at the carbon with the allylic hydroxyl group.[9] c) Outline of anti addition/anti elimination catalytic cycle identified with our previous DFT calculations.

Experiments to examine the mechanism of these Au- and Pd-catalyzed cyclization showed that both *cis* and *trans* allylic alcohols resulted in a *trans* alkene product (Scheme 1b).[9] Also, Aponick demonstrated that cyclization of chiral alcohols resulted in chirality transfer during alkoxylation carbon-oxygen bond formation. While there are multiple stepwise and concerted mechanisms that can account for these stereo-controlled reactions, our group previously showed with density functional theory (DFT) calculations that a two-step anti addition/anti elimination mechanism with a metal-alkyl intermediate is significantly lower than other mechanisms,[15,16] such as two-step syn addition/syn elimination or carbocation mechanisms.

The Au catalytic cycle outlined in Scheme 1c is based on the DFT potential energy surface shown in Scheme 2a.[15] During this catalytic cycle, hydrogen bonding between the hydroxyl groups preorganizes alkoxylation π-addition that occurs through **TS1**. This transition state connects to the anti addition Au-alkyl intermediate with hydrogen bonding intact, but no proton transfer. In the second step on this energy surface through **TS2** there is proton transfer along with water elimination to generate the new π bond.

An important mechanistic typical assumption for drawing the catalytic cycle in Scheme 1c is that after **TS1** there is fast intramolecular vibrational energy redistribution (IVR) and statistical vibrational population of the anti addition Au-alkyl intermediate prior to traversing **TS2**. Stated another way, based on the DFT potential energy surface, it is assumed there is fast equilibration between atomic potential and kinetic energy, so that after **TS1** the reaction pauses at intermediate **2** and has a significant lifetime before continuing through **TS2**. However, for the Au-catalyzed allylic diol cyclization reaction, the anti Au-alkyl intermediate is endothermic and only stabilized by ~2 kcal/mol relative to **TS1** and <1 kcal/mol relative to **TS2**. This relatively shallow well on the energy surface suggested to us that this reaction mechanism might be significantly influenced by atomic momenta and that a possible lack of IVR would lead to coupled reaction steps that skip the Au-alkyl intermediate during catalysis, which raises the general question of when a catalytic intermediate should be proposed based on DFT calculations. The dotted orange arrow in Scheme 2a depicts the possibility of dynamical motion and non-IVR resulting in the coupling of alkoxylation π-addition, proton transfer, and water elimination into a single reaction step.

Scheme 2b outlines this dynamical one-step mechanism on a More O'Ferrall-Jencks[17,18] type plot with axes for addition and elimination steps. Additionally, there is the possibility of proton transfer preceding alkoxylation carbon-oxygen bond formation.

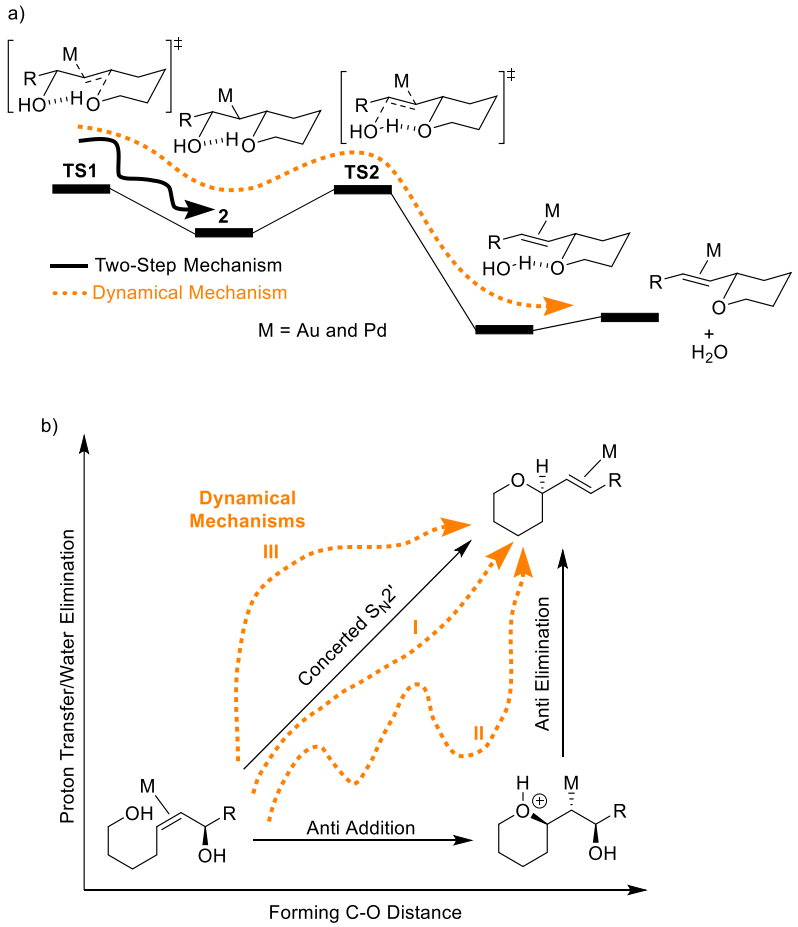

Scheme 2. a) Qualitative energy landscape based on previous DFT calculations depicting transition-state structures for the two-step anti addition/anti elimination mechanism.[15,16] b) More O'Ferrall-Jencks type plot comparing two-step (anti addition/anti elimination) and one-step, concerted S_N2' mechanisms. The orange dotted arrows (**I**, **II**, and **III**) represent several possible dynamical reaction mechanisms that couple addition and elimination reaction steps.

Here, we report DFT-based quasiclassical direct dynamics trajectories that determine the influence of atomic momenta during Au-catalyzed monoallylic diol cyclization reaction. Our trajectories demonstrate that for the shallow minimum energy surface with Au there is indeed extremely fast (ballistic) skipping of the Au-alkyl intermediate with dynamical coupling of addition, proton transfer, and elimination steps. We also examined the Pd-catalyzed diol cyclization reaction and found that the more

stabilized Pd-alkyl intermediate results in some trajectories with intermediate skipping and some trajectories ending at the intermediate. These results mean that interpretation of the Au- and Pd-catalyzed DFT potential-energy landscape is insufficient to propose a catalytic cycle. Consideration of atomic momenta through dynamics simulations is needed to determine if the Au-alkyl and Pd-alkyl intermediates are genuinely part of the catalytic cycle for monoallylic diol cyclization reactions.

DFT Calculations and Dynamics Simulations

DFT structures for energy landscapes were optimized in Gaussian 16[19] with the M06[20] functional using the 6-31G**[LANL2DZ for Au and Pd] basis set. This functional is one of the most accurate methods for properties of third-row transition metals. All structures were optimized with the ultrafine integration grid and with tight convergence criteria. Thermochemical corrections for enthalpies and Gibbs free energies were applied using the standard rigid rotor-harmonic oscillator approximation. Use of the quasi-harmonic oscillator approximation gave nearly identical energies. The continuum SMD dichloromethane solvent model was used for all optimizations.[21]

Trajectory calculations were initialized and propagated in Gaussian 16 with M06/6-31G**[LANL2DZ], an ultrafine integration grid, and the SMD dichloromethane solvent model. Quasiclassical trajectories that included zero-point energy (ZPE) were initialized and propagated from the anti addition transition-state structure **TS1**. Initialization of trajectories was done using local mode and thermal sampling at 298 K. The Au-catalyzed and Pd-catalyzed reactions both showed very high conversion at and below room temperature.[9,13] Trajectories were propagated in mass-weighted Cartesian velocities with an average step size of about 0.75 fs, which we previously showed is a reasonable time step for organometallic reactions.[22,23] Forward trajectories were initiated so that the transition-state vibrational mode was followed in the direction of decreasing the forming C-O bond length. Reverse trajectories followed the direction of increasing this C-O bond length.

Results and Discussion

DFT potential energy landscapes with transition-state and intermediate structures are very often used to analyze catalytic organometallic reaction mechanisms and propose catalytic cycles. A general assumption in the interpretation of energy landscapes, based on transition state theory[24,25,26] and other statistical theories, is that transition-state and intermediate static structures represent an average of an ensemble. Moreover, intermediate structures have atomic kinetic energy in an equilibrium distribution among harmonic vibrational modes and that at an intermediate there is IVR, which results in a significant lifetime of the intermediate.[27,28]

For organic reactions there are now several studies showing that atomic momenta impact the reaction mechanism, selectivity, and lifetime of intermediates.[29,30,31,32,33,34,35,36,37] Recently, we discovered dynamic effects in a few stoichiometric organometallic reactions. For example, in the C-H activation between methane and $[Cp^*(PMe_3)Ir^{III}(CH_3)]^+$,[38] as well as the β-hydrogen transfer for $[Cp^*Rh^{III}(Et)(ethylene)]^+$,[39] despite a fully characterized intermediate on the DFT-potential energy landscape, direct dynamics simulations revealed that the intermediate is either sometimes or always skipped due to dynamical coupling of multiple reaction steps through dynamic matching or the lack of IVR. We also discovered dynamic effects, specifically dynamical pathway branching, in the reaction between $Tp(NO)(PR_3)W$ and benzene[40] as well as $Cp(PMe_3)_2Re$ and ethylene.[41] Related organometallic dynamic effects were reported for hydrogenation reaction steps of $(Cl)(CO)(PH_3)Ru^{II}(H)(H_2)(C_2H_4)$,[42] Rh-carbenoid C-H bond insertion,[43] and Au/Ag arene C-H functionalization.[44] There are also recent reports of dynamic effects for Ru geminal hydroboration,[45] Fe Diels-Alder reactions,[46] Fe arene amination,[47] and Pd transmetallation.[48]

Quasiclassical direct dynamics trajectories allow examination of reaction mechanisms beyond characterization of the potential energy surface because there is inclusion of atomic kinetic energy. More specifically, in a DFT quasiclassical direct dynamics simulation zero-point and temperature-dependent vibrational energy is added to the transition-state structure in the form of both kinetic and potential energy. The structure is then propagated over time using classical equations of motion with atomic forces

solved at each step directly by using DFT. This type of simulation provides the timing of geometry changes and lifetime of intermediates, which is not available from the DFT potential-only energy landscape and intrinsic reaction coordinate (IRC) calculations that have infinitesimal atomic velocity.[49]

To begin, we calculated the Au and Pd energy surfaces using M06 DFT (Scheme 3). Similar to our previous reports,[15,16] we located alkoxylation anti addition transition state **TS1**, the Au-alkyl and Pd-alkyl intermediates (**2**), and the proton transfer/anti elimination transition state **TS2**. For both Au and Pd, in **TS1** there is the intramolecular hydrogen bonding that controls stereochemistry. This transition state only involves carbon-oxygen bond formation. IRC calculations confirm the connection of **TS1** to **2** on the energy surface and show that the hydrogen bond interaction is slightly enhanced, but there is no intramolecular proton transfer. In **TS2** the proton transfer is nearly complete and allows elimination of water and change of an alkyl-metal intermediate back to π coordination. IRC calculations confirm that **TS2** involves both proton transfer and water elimination. Based on these energy surfaces, both Au and Pd reactions have the same catalytic cycle that is outlined in Scheme 1c.

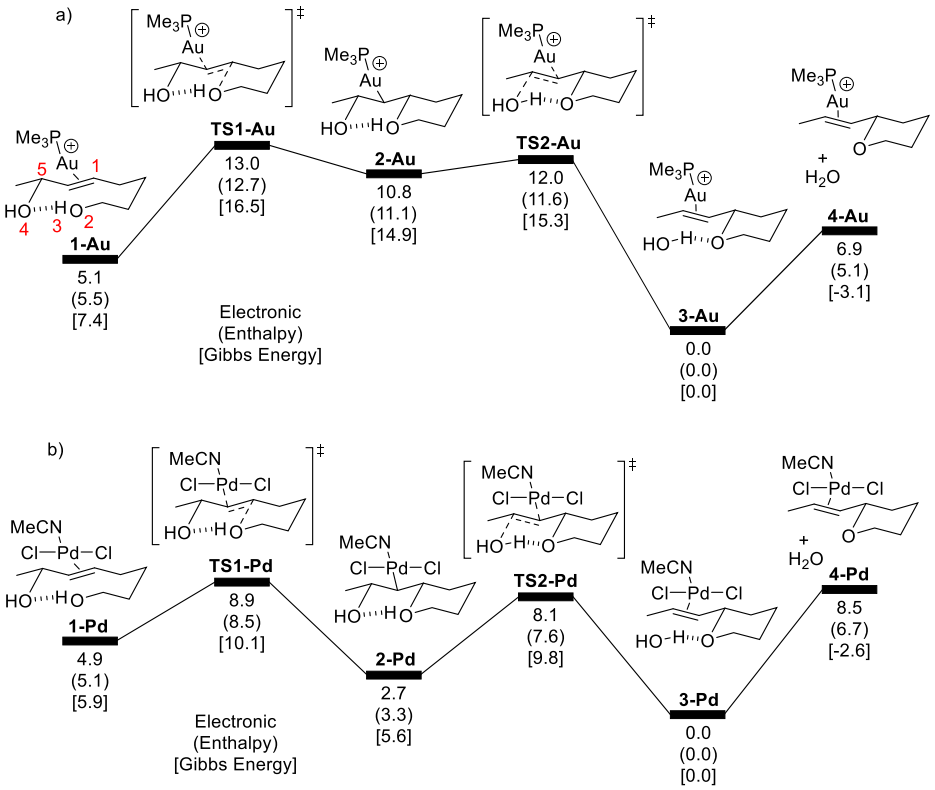

Scheme 3. M06/6-31G**[LANL2DZ for Au] energy landscape for a) the Au-catalyzed monoallylic diol cyclization reaction at 298 K and b) Pd-catalyzed monoallylic diol cyclization reaction at 298 K. Red numbers in structure **1-Au** define atom numbering. (kcal/mol)

For the Au reaction (Scheme 3a), while the Au-alkyl intermediate **2-Au** is assumed to be formed during catalysis, it is endothermic and only stabilized by 1.6 kcal/mol relative to **TS1-Au** and 0.5 kcal/mol relative to **TS2-Au** on the enthalpy surface. Therefore, **2-Au** resides in a shallow well on the enthalpy and Gibbs energy landscapes and the formation and lifetime of this intermediate is likely significantly influenced by atomic momenta after **TS1-Au**. We have confirmed this shallow well with DLPNO-CCSD(T)/def-TZVP calculations in ORCA,[50] which only gives an intermediate stabilized by slightly more than 1.5 kcal/mol.

There are several possible ways that atomic momenta can impact this mechanism. First, it is possible that the reaction coordinate motion leaving **TS1-Au** is coupled/matched with proton transfer leading to **TS2-Au**. In this case, which is outlined as the dotted orange arrow **I** in Scheme 2b, there would be extremely rapid/ballistic traversing of the Au-alkyl intermediate without stopping and the addition and

elimination steps are merged into a single dynamical one-step mechanism.[31,32] Second, it is possible that intermediate **2-Au** is formed, but without rapid and complete IVR. This would result in the relatively brief sampling on intermediate **2** followed by proton transfer and water elimination. This mechanistic scenario is outlined by the dotted orange arrow **II** in Scheme 2b. Previously, we referred to this type of mechanism as dynamically unrelaxed.[39] Third, there is the possibility where proton transfer precedes carbon-oxygen bond formation (Scheme 2b orange dotted arrow **III**). Similar to this suggestion, Singleton found that a proton can dynamically transfer before carbon-carbon bond cleavage during benzoylacetic acid decarboxylation.[51] Last, there is the possibility that complete IVR occurs, and **2-Au** is formed in what would be best classified as a two-step addition/elimination mechanism.

To examine these dynamical mechanism possibilities, we initiated and propagated 95 Au trajectories starting from **TS1-Au**. Figure 1 displays these trajectories with color coding. Red lines represent recrossing trajectories that turnaround and proceed back through **TS1-Au**. Recrossing can be substantial on a relatively flat surface. Consistent with this idea, 47 out of 95 trajectories (49.5%) recrossed **TS1-Au**. Recrossing is most apparent by tracking the forming carbon-oxygen bond, C1-O2 (Figure 1a). Interestingly, there is a band of very fast recrossing trajectories where within 50 fs there is initial motion towards **2-Au** followed by very fast turnaround. There are also several recrossing trajectories where **2-Au** is formed, but due to the lack of IVR there is rebound back to **TS1-Au**.

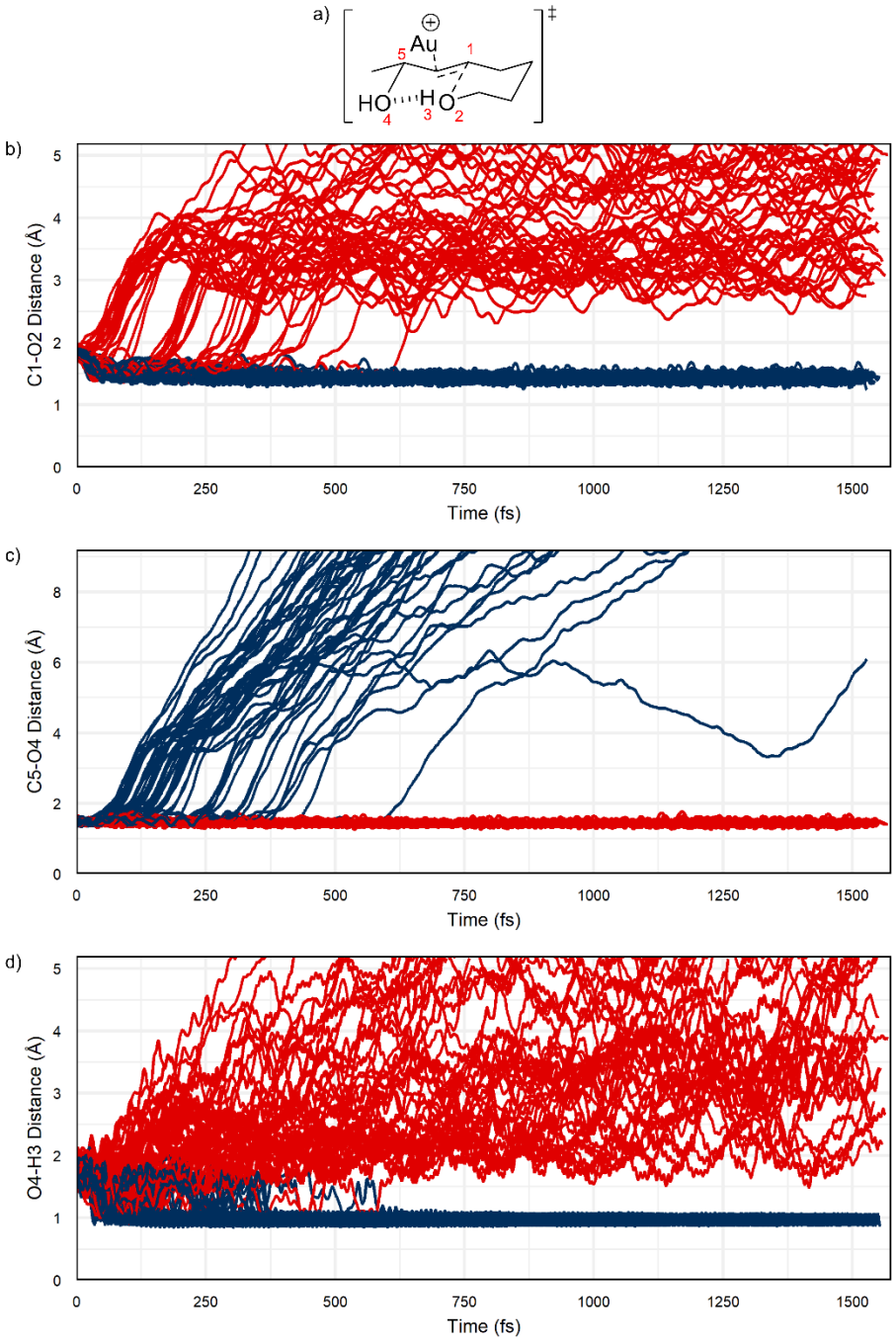

Figure 1. Plots tracking distances (in Å) versus time (in fs) for 95 Au-catalyzed trajectories initiated at **TS1-Au** (a) and progressing forward towards **2-Au**. b) Tracking formation of the carbon-oxygen bond (C1-O2), c) breaking carbon-oxygen bond (C5-O4), and d) forming oxygen-hydrogen bond (O4-H3) for proton transfer. Blue lines represent trajectories with long C5-O4 distances and indicate progression beyond **2-Au** (48 trajectories, 50.5%). Red lines represent recrossing trajectories that return to **1-Au** (47 trajectories, 49.5%). No trajectories remained at intermediate **2** after 750 fs.

In Figure 1 blue lines represent trajectories that descend from **TS1-Au** towards intermediate **2-Au**, but ultimately progress to **TS2-Au** and beyond. Figures 1b and 1c track the breaking carbon-oxygen bond (C5-O4) and the forming oxygen-hydrogen bond (O4-H3) for proton transfer. These plots reveal that all non-recrossing trajectories from **TS1-Au** skip intermediate **2-Au** and lead to intermediate **3-Au** with complete proton transfer and water elimination. Importantly, Figure 1b reveals that nearly all blue trajectories show extremely fast, ballistic traversing of intermediate **2-Au** between 50 and 200 fs where **TS1-Au** is to a large extent dynamically coupled with **TS2-Au**, which was outlined by the dotted orange arrow **I** in Scheme 2b. Figure 2a shows images along a representative ballistic trajectory. From the transition state with time labeled at 0 fs, by 29 fs the new C-O bond is fully formed and by 57 fs the proton is transferred. Only 30 fs later water begins to dissociate and by 113 it is completely gone from the newly formed alkene unit. Based on these ballistic trajectories, in contrast to the two-step mechanism based on the DFT potential energy landscape, inclusion of atomic momenta show that addition, proton transfer, and elimination occur in a single reaction process. This indicates that it may not be appropriate for the Au-alkyl intermediate to be proposed as an intermediate in the catalytic cycle for Au-catalyzed allylic diol cyclization.

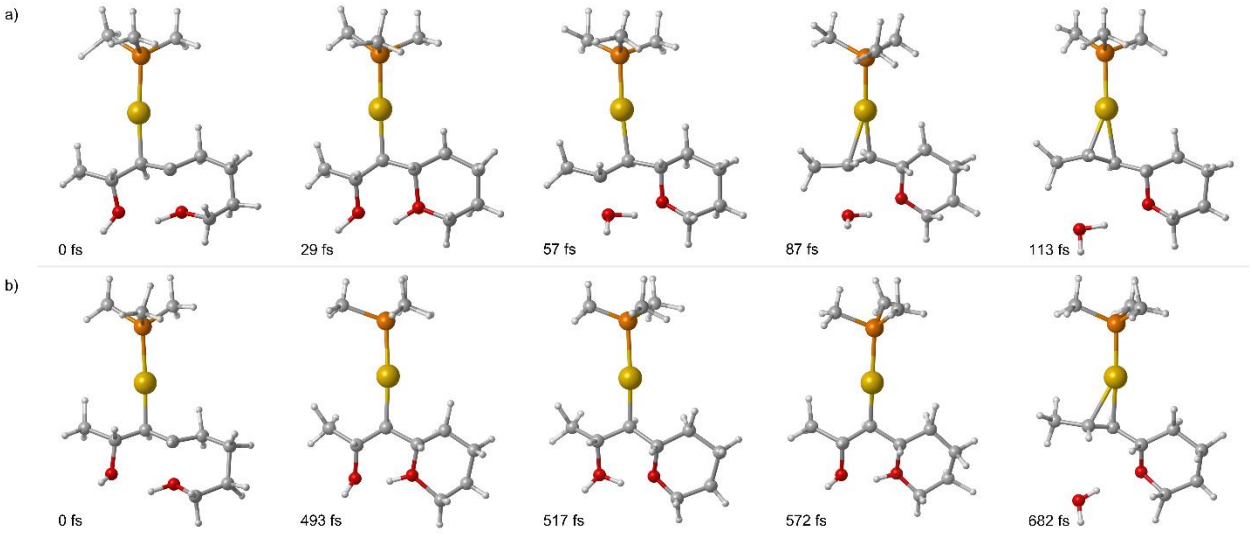

Figure 2. Snapshots from representative trajectories initiated at **Au-TS1** that illustrate a) ballistic motion and a dynamically concerted mechanism and b) unrelaxed trajectory with proton ping pong.

In addition to the many ballistic trajectories, there are also a few trajectories that sample intermediate **2-Au** for up to ~450 fs before proceeding through **TS2-Au** and onto **3-Au**. These are perhaps best categorized as unrelaxed trajectories where there is incomplete IVR. We did not find any trajectories that showed proton transfer prior to carbon-oxygen bond formation. This in retrospect is probably reasonable considering that proton transfer between neutral hydroxyl groups is extremely endothermic and that proton transfer only occurs after alkoxylation promoted by Au. While proton transfer does not proceed prior to carbon-oxygen bond formation, comparison of the timing of proton transfer with carbon-oxygen bond cleavage/water elimination does show that these two processes are dynamically coupled in both ballistic and unrelaxed trajectories. Figure 3 shows histograms for timing of the forming C-O bond, breaking C-O bond, and breaking O-H bond for the 48 non-recrossing trajectories. There was an average difference of 20 fs between C-O bond formation and C-O cleavage with the longest difference being 55 fs. Typically, carbon-oxygen bond cleavage occurs within 10 fs of proton transfer.

We also found that for the non-ballistic, unrelaxed trajectories that skip intermediate **2-Au** there is the possibility of proton ping pong between the hydroxyl groups prior to water elimination. Figure 1c displays several blue line trajectories where the forming O-H bond first becomes short at about 1.0 Å, but then increases to >1.5 Å that is closer to the distance in intermediate **2-Au**. On average there are three proton oscillations between hydroxyl groups prior to water elimination. Figure 2b shows images along a representative ping pong trajectory. From the transition state (0 fs), the new C-O bond is formed at about 493 fs. 24 fs later, at 517 fs after the transition state, the proton is transferred to the other hydroxyl group. 55 fs later, at 572 fs, the proton moves back to the first hydroxyl group. At 682 fs the proton goes back to the second hydroxyl group and this time the proton transfer is coupled to water elimination.

Importantly, for a Au-catalyzed process this is the first time that trajectories have revealed nonstatistical dynamic skipping of an intermediate and the coupling of several reaction steps into a single process. In a few previous studies with Au catalysis, trajectories or analysis of the potential energy surface revealed the different dynamic effect of a post-transition state pathway bifurcation.[52,53,54,55,56] This

new discovery will impact the interpretation of several experimental and computational studies that propose multi-step catalytic reaction mechanisms involving Au-alkyl or Au-vinyl intermediates after π-bond addition.[57]

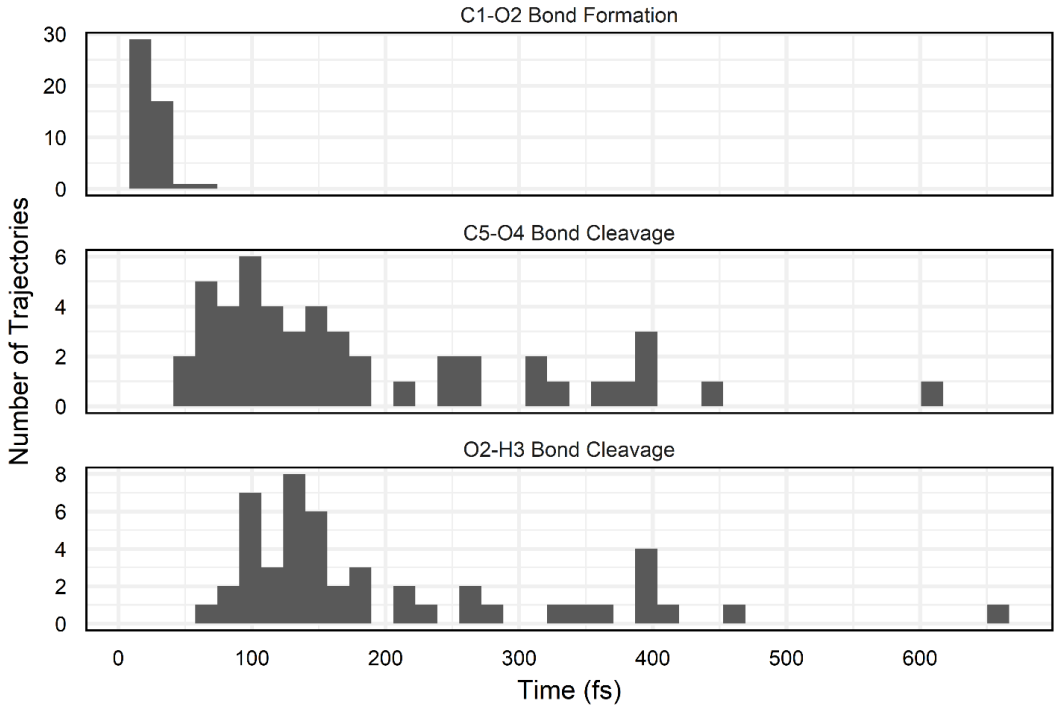

Figure 3. Histograms showing the timing of key bond formations and cleavages of 48 non-recrossing Au-catalyzed trajectories initiated at **TS1-Au** and progressing forward towards **2-Au**.

While the energy landscapes in Schemes 3a and 3b both show two steps that involve first π-bond addition and second proton transfer/water elimination there is a potentially important difference in the relative energies of the Au-alkyl and Pd-alkyl intermediates. On the Au surface, intermediate **2-Au** is only slightly stabilized compared to **TS1-Au** and **TS2-Au** whereas on the Pd surface **2-Pd** is 4-6 kcal/mol lower in energy than **TS1-Pd** and **TS2-Pd**, depending on the analysis of either the electronic or Gibbs surfaces. In our effort to understand how the qualitative and quantitative shape of a DFT potential energy surface relates to mechanisms that include dynamical motion,[39] we wanted to know if this more stabilized Pd-alkyl intermediate is dynamically skipped akin to the Au reaction or if it is stable enough to result in a

genuine intermediate with substantial IVR. Therefore, we initiated and propagated 84 Pd trajectories beginning at **TS1-Pd**.

Figure 4 displays plots of these 84 Pd trajectories as a function of time and forming and breaking C-O bonds and forming O-H bond. With a deeper energy well for intermediate **2-Pd**, and an overall less flat energy surface, the amount of recrossing is less, but still substantial at 32% (27 out of 84 trajectories, red line trajectories in Figure 4). Figure 4b best illustrates the types of trajectories found for Pd. In addition to red recrossing trajectories, we also found intermediate **2-Pd** skipping trajectories labeled with blue lines. However, in contrast to the Au reaction, we also found non-skipping trajectories labeled as green lines. In contrast to all trajectories skipping during Au catalysis, the majority of non-recrossing trajectories did not skip and ended at **2-Pd** (37 our 84 trajectories). There were some skipping trajectories (20 out of 84 trajectories). These skipping trajectories are best classified as unrelaxed skipping rather than ballistic trajectories. Figure 4b shows that no trajectories skipped the Pd-alkyl intermediate until after 150 fs. Similar to the unrelaxed Au trajectories, the unrelaxed Pd trajectories showed proton ping pong between hydroxyl groups prior to water elimination. On average, there were two complete back-and-forth proton movements before water elimination.

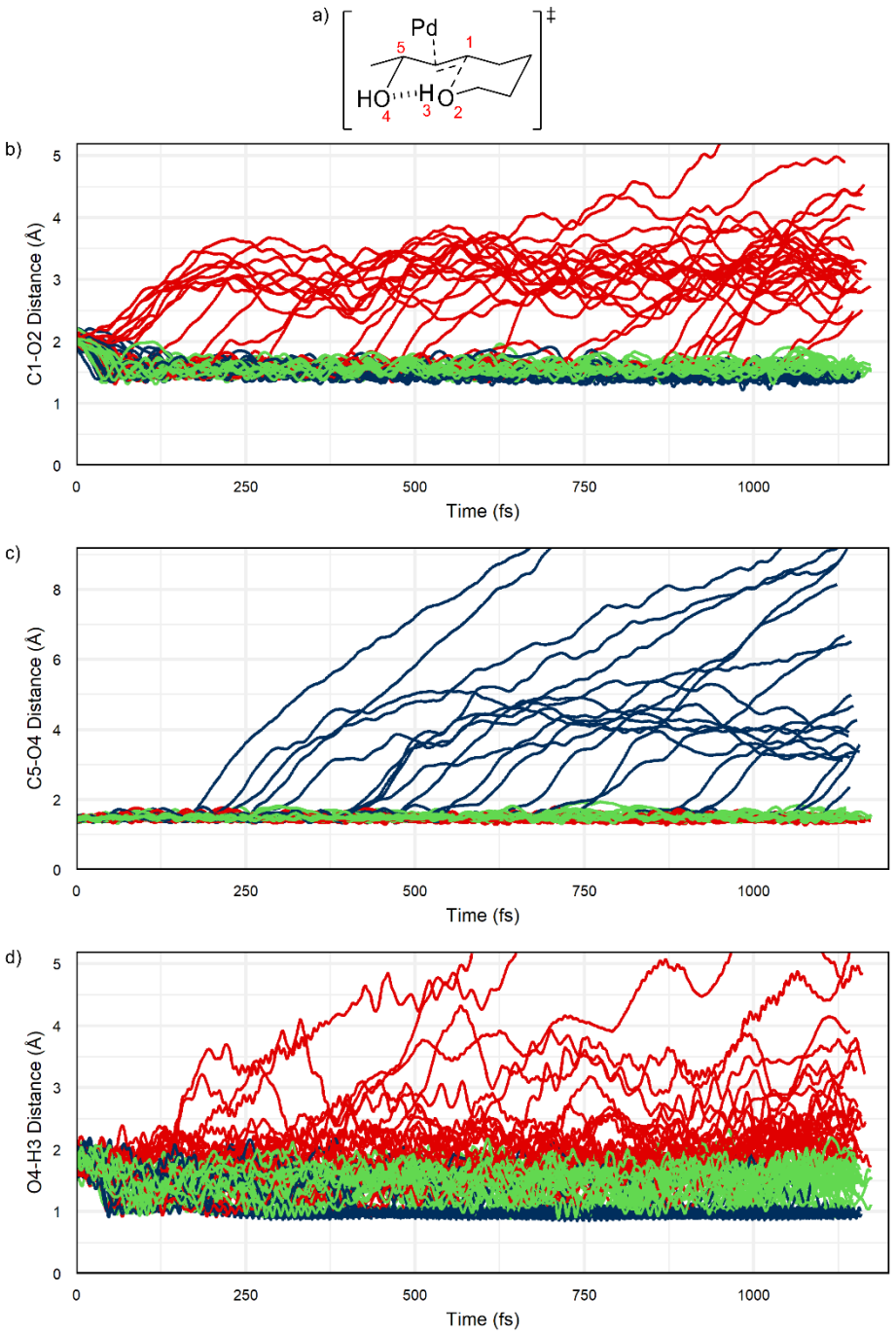

Figure 4. Plots of tracking distances (in Å) versus time (in fs) for 84 Pd-catalyzed trajectories initiated at **TS1-Pd** (a) and progressing forward towards **2-Pd**. b) Tracking formation of the carbon-oxygen bond (C1-O2), c) breaking carbon-oxygen bond (C5-O4), and d) breaking oxygen-hydrogen bond (O4-H3) for proton transfer. Green lines represent trajectories that do not progress beyond **2-Pd**, which is consistent with a two-step mechanism (37 trajectories, 44.0%). Blue lines represent trajectories with long C5-O4 distances and indicate progression beyond **2-Pd** (20 trajectories, 23.8%). Red lines represent recrossing trajectories that return to **1-Pd** (27 trajectories, or 32.1%).

Conclusions

Using quasiclassical direct dynamics simulations, new dynamical mechanisms were revealed for Au- and Pd-catalyzed allylic diol cyclization. For Au, ballistic trajectories revealed extremely fast skipping of a Au-alkyl intermediate during the anti addition/anti elimination process (blue dotted arrow in Scheme 4a). Additionally, a somewhat slower, but still mechanistically coupled, unrelaxed dynamical mechanism was also found that involves brief sampling of the Au-alkyl intermediate before proceeding to the elimination step (red dotted arrow in Scheme 4a). These dynamical mechanisms show that addition, proton transfer, and elimination occur can occur in single reaction process. In contrast to Au catalysis, for Pd catalysis, due a more stabilized Pd-alkyl intermediate, only about half of trajectories show Pd-alkyl intermediate skipping through an unrelaxed dynamical mechanism and no ballistic trajectories were identified. The other half of the trajectories show the traditional two-step mechanism with a much longer-lasting Pd-alkyl intermediate.

This work demonstrated that interpretation of DFT calculated potential-energy landscape for catalytic cycles can be incomplete without consideration of atomic momenta. Typically, when catalytic cycles are outlined based on DFT calculations intermediates are drawn for each major minimum energy structure regardless of the surface shape. Importantly, one of the many implications of drawing a structure on a catalytic cycle is the potential of direct observation or interception of this intermediate. For this allylic diol cyclization, Schemes 4b and 4c show updated catalytic cycles based on these dynamical mechanisms. For example, in Scheme 4b, some of the trajectories leave the π-coordination intermediate and through a ballistic mechanism lead directly the cyclized pyran product. There are also other trajectories that briefly sample the Au-alkyl intermediate before generating the pyran. None of the trajectories show the full catalytic cycle where the Au-alkyl has a long lifetime. Scheme 4c shows that the Pd catalysis involves both the full catalytic cycle as well as the unrelaxed dynamical mechanism.

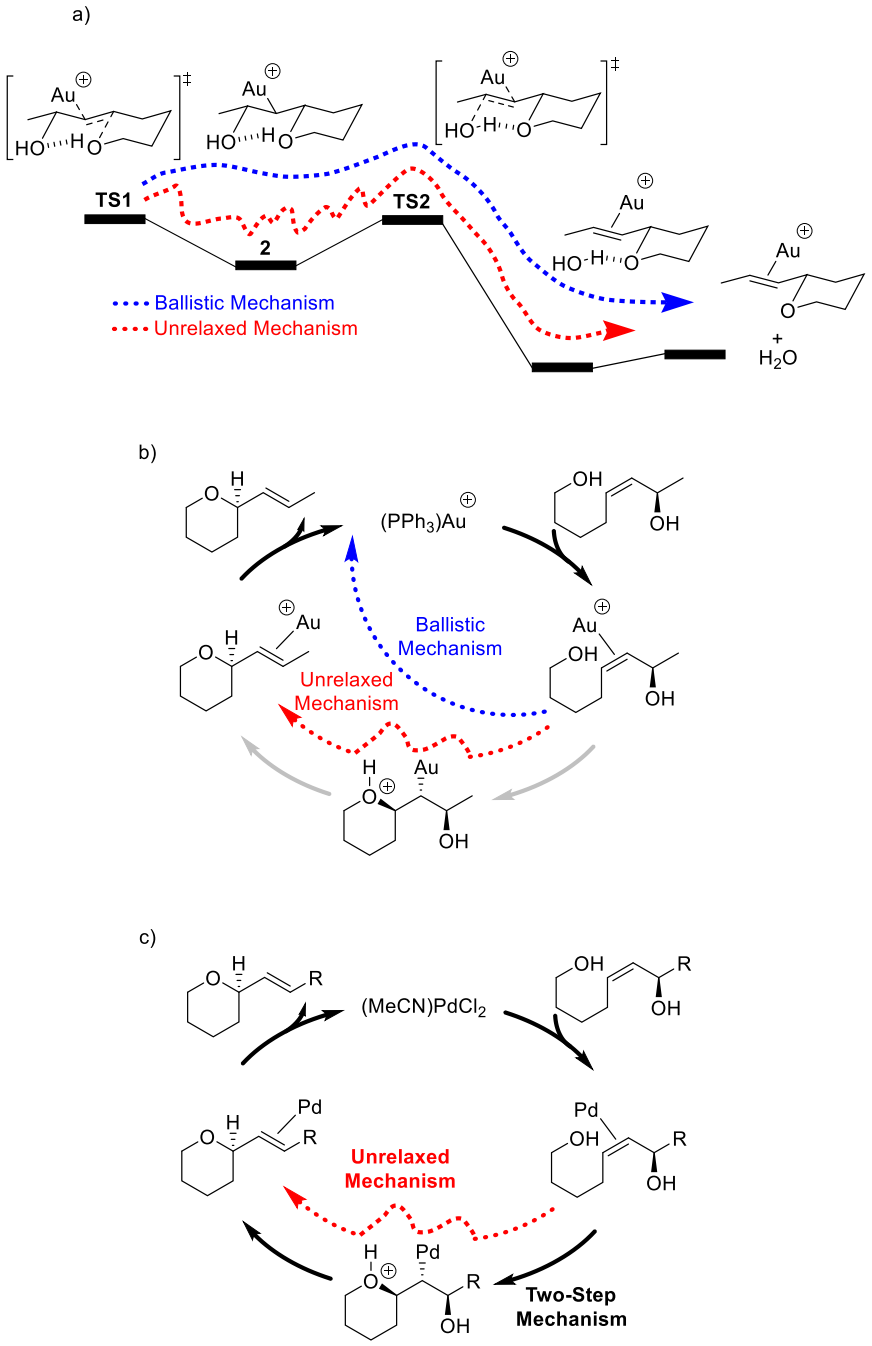

Scheme 4. a) Qualitative Au-catalyzed potential energy landscape depicting structures for the two-step anti addition/anti elimination mechanism. The dotted blue arrow depicts the dynamical ballistic reaction mechanism. The dotted red arrow depicts the dynamical unrelaxed mechanism. b) Updated Au catalytic cycle that incorporates ballistic and unrelaxed mechanisms. c) Updated Pd catalytic cycle that incorporates the unrelaxed dynamical mechanism.

Supporting Information

Xyz structures and initial trajectory configurations. This information is available free of charge on the ACS Publications website.

Acknowledgments

We thank Brigham Young University and the Office of Research Computing, especially the Fulton Supercomputing Lab.

Corresponding Author

*dhe@chem.byu.edu

Funding Sources

D.H.E. acknowledges the United States National Science Foundation Chemical Structure, Dynamics, and Mechanisms B (CSDM-B) Program for support under award CHE 1952420. M.S.T. and W.S. thank the BYU Department of Chemistry and Biochemistry for undergraduate research awards.

Conflict of Interest

There are no conflicts of interest to declare.

References

1. Leyva-Pėrez, A.; Sabater, M. J. Gold-catalyzed carbon− heteroatom bond-forming reactions. *Chem. Rev.* **2011**, *111*, 1657−1712.

2. Hosokawa, T.; Murahashi, S.-I. Intramolecular Oxypalladation. In Handbook of Organopalladium Chemistry for Organic Synthesis; Negishi, E.-i., Ed.; John Wiley and Sons: New York, 2002; Vol. 2, pp 2169−2192.

3. Fürstner, A.; Davies, P. W. Catalytic Carbophilic Activation: Catalysis by Platinum and Gold π Acids. *Angew. Chem., Int. Ed.* **2007**, *46*, 3410−3449.

4. Fürstner, A. Gold and platinum catalysis—a convenient tool for generating molecular complexity. *Chem. Soc. Rev.* **2009**, *38*, 3208−3221.

5. Hashmi, A. S. K. Homogeneous gold catalysis beyond assumptions and proposals—characterized intermediates. *Angew. Chem., Int. Ed.* **2010**, *49*, 5232-5241.

6. Liu, L.-P.; Hammond, G. B. Recent advances in the isolation and reactivity of organogold complexes. *Chem. Soc. Rev.* **2012**, *41*, 3129−3139

7. Widenhoefer, R. A.; Song, F.; Edited by Yudin, A. K. Gold-catalyzed addition of oxygen nucleophiles to C-C multiple bonds. From Catalyzed Carbon-Heteroatom Bond Formation, 2011, 463−492.

8. Lalonde, R. L.; Brenzovich, W. E., Jr.; Benitez, D.; Tkatchouk, E.; Keley, K.; Goddard, W. A.; Toste, F. D. Alkyl gold complexes by the intramolecular aminoauration of unactivated alkenes. *Chem. Sci.* **2010**, *1*, 226−233

9. Aponick, A.; Li, C.-Y.; Biannic, B. A. Au-catalyzed cyclization of monoallylic diols. *Org. Lett.* **2008**, *10*, 669−671.

10. Aponick, A.; Biannic, B. Gold-catalyzed dehydrative cyclization of allylic diols. *Synthesis* **2008**, *20*, 3356−3359

11. Aponick, A.; Li, C.-Y.; Malinge, J.; Marques, E. F. An extremely facile synthesis of furans, pyrroles, and thiophenes by the dehydrative cyclization of propargyl alcohols. *Org. Lett.* **2009**, *11*, 4624−4627.

12. Ketcham, J. M.; Biannic, B.; Aponick, A. The tandem intermolecular hydroalkoxylation/claisen rearrangement *Chem. Commun.* **2013**, *49*, 6849–4159.

13. Uenishi, J.; Ohmi, M.; Ueda, A. PdII-Catalyzed stereospecific formation of tetrahydro-and 3,6-dihydro[2H]pyran rings: 1,3-chirality transfer by intramolecular oxypalladation reaction. *Tetrahedron: Asymmetry* **2005**, *16*, 1299−1303.

14. Kawai, N.; Lagrange, J.-M.; Ohmi, M.; Uenishi, J. Palladium-catalyzed stereospecific synthesis of 2,6-disubstituted tetrahydropyrans: 1,3-chirality transfer by an intramolecular oxypalladation reaction. *J. Org. Chem.* **2006**, *71*, 4530−4537.

15. Ghebreghiorgis, T.; Biannic, B.; Kirk, B. H.; Ess, D. H.; Aponick, A. The importance of hydrogen bonding to stereoselectivity and catalyst turnover in gold-catalyzed cyclization of monoallylic diols. *J. Am. Chem. Soc.* **2012**, *134*, 16307−16318.

16. Ghebreghiorgis, T.; Biannic, B.; Kirk, B. H.; Aponick, A.; Ess, D. H.; Multiple Mechanisms in Pd(II)-Catalyzed S_N2' Reactions of Allylic Alcohols *J. Org. Chem.* **2013**, *78*, 7664−7673.

17. More O'Ferrall, R. A. Relationships between E2 and E1cB mechanisms of β-elimination. *J. Chem. Soc. B* **1970**, 274−277.

18. Jencks, W. P. General acid-base catalysis of complex reactions in water. *Chem. Rev.* **1972**, *72*, 705−718.

19. Frisch, M. J.; Trucks, G. W.; Schlegel, H. B.; Scuseria, G. E.; Robb, M. A.; Cheeseman, J. R.; Scalmani, G.; Barone, V.; Petersson, G. A.; Nakatsuji, H.; Li, X.; Caricato, M.; Marenich, A. V.; Bloino, J.; Janesko, B. G.; Gomperts, R.; Mennucci, B.; Hratchian, H. P.; Ortiz, J. V.; Izmaylov, A. F.; Sonnenberg, J. L.; Williams-Young, D.; Ding, F.; Lipparini, F.; Egidi, F.; Goings, J.; Peng, B.; Petrone, A.; Henderson, T.; Ranasinghe, D.; Zakrzewski, V. G.; Gao, J.; Rega, N.; Zheng, G.; Liang, W.; Hada, M.; Ehara, M.; Toyota, K.; Fukuda, R.; Hasegawa, J.; Ishida, M.; Nakajima, T.; Honda, Y.; Kitao, O.; Nakai, H.; Vreven, T.; Throssell, K.; Montgomery Jr., J. A.; Peralta, J. E.; Ogliaro, F.; Bearpark, M. J.; Heyd, J. J.; Brothers, E. N.; Kudin, K. N.; Staroverov, V. N.; Keith, T. A.; Kobayashi, R.; Normand, J.; Raghavachari, K.; Rendell, A. P.; Burant, J. C.; Iyengar, S. S.; Tomasi, J.; Cossi, M.; Millam, J. M.; Klene, M.; Adamo, C.; Cammi, R.; Ochterski, J. W.; Martin, R. L.; Morokuma, K.; Farkas, O.; Foresman, J. B.; Fox, D. J. Gaussian 16, revision B.01; Gaussian, Inc., Wallingford CT, 2016.

20. Zhao, Y.; Truhlar, D. G. The M06 Suite of Density Functionals for Main Group Thermochemistry, Thermochemical Kinetics, Noncovalent Interactions, Excited States, and Transition Elements: Two New

Functionals and Systematic Testing of Four M06-Class Functionals and 12 Other Functionals. *Theor. Chem. Acc.* **2008**, *120*, 215–241.

21. Marenich, A. V.; Cramer, C. J.; Truhlar, D. G. Universal Solvation Model Based on Solute Electron Density and on a Continuum Model of the Solvent Defined by the Bulk Dielectric Constant and Atomic Surface Tensions. *J. Phys. Chem. B* **2009**, *113*, 6378–6396.

22. Carlsen, R.; Jenkins, J. R.; Ess, D. H. Molecular Dynamics Analysis of the Cationic Cp*(PMe_3)Ir(CH_3) Methane C-H Activation Mechanism. *Faraday Discussions*, **2019**, *220*, 414–424.

23. Teynor, M. S.; Carlsen, R.; Ess, D. H. Relationship Between Energy Landscape Shape and Dynamics Trajectory Outcomes for Methane C-H Activation by Cationic Cp*(PMe_3)Ir/Rh/Co(CH_3). *Organometallics*, **2020**, *39*, 1393–1403.

24. Eyring, H. The Activated Complex in Chemical Reactions. *J. Chem. Phys.* **1935**, *3*, 107–115.

25. Laidler, K. J.; King, M. C. Development of transition-state theory. *J. Phys. Chem.* **1983**, *87*, 2657–2664.

26. Truhlar, D. G.; Garrett, B. C.; Klippenstein, S. J. Current Status of Transition-State Theory. *J. Phys. Chem.* **1996**, *100*, 12771–12800.

27. Ma, X.; Hase, W. L. Perspective: Chemical Dynamics Simulations of Non-Statistical Reaction Dynamics. *Phil. Trans. R. Soc. A* **2017**, *375*, 20170035.

28. Lourderaj, U.; Park, K.; Hase, W. L. Classical Trajectory Simulations of Post-Transition State Dynamics. *Int. Rev. Phys. Chem.* **2009**, *113*, 2236–2253.

29. Paranjothy, M.; Sun, R.; Zhuang, Y.; Hase, W. L. Direct Chemical Dynamics Simulations: Coupling of Classical and Quasiclassical Trajectories with Electronic Structure Theory. *Wiley Interdiscip. Rev. Comput. Mol. Sci.* **2013**, *3*, 296–316.

30. Carpenter, B. K. Nonstatistical Dynamics in Thermal Reactions of Polyatomic Molecules. *Annu. Rev. Phys. Chem.* **2005**, *56*, 57–89.

31. Carpenter, B. K. Energy Disposition in Reactive Intermediates *Chem. Rev.* **2013**, *113*, 7265–7286.

32. Carpenter, B. K. Potential Energy Surfaces and Reaction Dynamics. In *Reactive Intermediate Chemistry*; Moss, R. A.; Platz, M. S.; Jones, M. Jr., Eds.; John Wiley & Sons, Inc.: New Jersey, 2004; pp 925–960.

33. Lopez, J. G.; Vayner, G.; Lourderaj, U.; Addepalli, S. V.; Kato, S.; de Jong, W. A.; Windus, T. L.; Hase, W. A. A Direct Dynamics Trajectory Study of F^- + CH_3OOH Reactive Collisions Reveals a Major Non-IRC Reaction Path. *J. Am. Chem. Soc.* **2007**, *129*, 9976–9985.

34. Doubleday, C.; Li, G.; Hase, W. L. Dynamics of the Biradical Mediating Vinylcyclopropane-Cyclopentene Rearrangement. *Phys. Chem. Chem. Phys.* **2002**, *4*, 304–312.

35. Bekele, T.; Christian, C. F.; Lipton, M. A.; Singleton, D. A. "Concerted" Transition State, Stepwise Mechanism. Dynamics Effects in C^2-C^6 Enyne Allene Cyclizations. *J. Am. Chem. Soc.* **2005**, *127*, 9216–9223.

36. Chen, Z.; Nieves-Quinones, Y.; Waas, J. R.; Singleton, D. A. Isotope Effects, Dynamic Matching, and Solvent Dynamics in a Wittig Reaction. Betaines as Bypassed Intermediates. *J. Am. Chem. Soc.* **2014**, *136*, 13122–13125.

37. Biswas, B.; Singleton, D. A. Controlling Selectivity by Controlling the Path of Trajectories. *J. Am. Chem. Soc.* **2015**, *137*, 14244–14247.

38. Carlsen, R.; Wohlgemuth, N.; Carlson, L.; Ess, D. H. Dynamical Mechanism May Avoid High-Oxidation State Ir(V)-H Intermediate and Coordination Complex in Alkane and Arene C-H Activation by Cationic Ir(III) Phosphine. *J. Am. Chem. Soc.* **2018**, *140*, 11039–11045.

39. Wheeler, J.; Carlsen, R.; Ess, D. H. Mechanistic Molecular Motion of Transition-Metal Mediated β-Hydrogen Transfer: Quasiclassical Trajectories Reveal Dynamically Ballistic, Dynamically Unrelaxed, Two Step, and Concerted Mechanisms. *Dalton Trans.* **2020**, *49*, 7747–7757.

40. Smith, J. A.; Schouten, A.; Wilde, J. H.; Westendorff, K. S.; Dickie, D. A.; Ess, D. H.; Harmen, W. D. Experiments and Direct Dynamics Simulations Reveal a Network of Reaction Pathways for Tungsten η^2-Arene - Aryl Hydride Equilibria. *J. Am. Chem. Soc.* **2020**, *142*, 16437–16454.

41. Yang, B.; Schouten, A.; Ess, D. H. Direct Dynamics Trajectories Reveal Nonstatistical Coordination Intermediates and Demonstrate that σ and π-Coordination are Not Required for Rhenium(I)-Mediated Ethylene C–H Activation. *J. Am. Chem. Soc.* **2021**, *143*, 8367–8374.

42. Rowley, C. N.; Woo, T. K. A Path Sampling Study of Ru-Hydride-Catalyzed H_2 Hydrogenation of Ethylene. *J. Am. Chem. Soc.* **2008**, *130*, 7218–7219.

43. Hare, S. R.; Tantillo, D. J. Cryptic post-transition state bifurcations that reduce the efficiency of lactone-forming Rh-carbenoid C–H insertions. *Chem. Sci.*, **2017**, *8*, 1442–1449.

44. Fructos, M. R.; Besora, M.; Braga, A. A. C.; Díaz-Requejo, Maseras, F.; Pérez, P. J. Mechanistic studies on gold-catalyzed direct arene C–H bond functionalization by carbene insertion: the coinage-metal effect. *Organometallics* **2017**, *36*, 172–179.

45. Feng, Q.; Wu, H.; Li, X.; Song, L.; Ghung, L. W.; Wu, Y-D.; Sun, J. Ru-Catalyzed Geminal Hydroboration of Silyl Alkynes via a New gem-Addition Mechanism. *J. Am. Chem. Soc.* **2020**, *142*, 13867–13877.

46. Unusual KIE and dynamics effects in the Fe-catalyzed hetero-Diels-Alder reaction of unactivated aldehydes and dienes. Yang, Y.; Zhang, X. Zhong, L-P.; Lan, J.; Li, C-C.; Chung, L. W. *Nat. Commun.* **2020**, *11*, 1850.

47. Li, B.; Li, Y.; Dang, Y.; Houk, K. N. Post-Transition State Bifurcation in Iron-Catalyzed Arene Aminations. *ACS Catal.* **2021**, *11*, 6816–6824.

48. Pu, M.; Sanhueza, I. A.; Senol, E.; Schoenebeck, F. Divergent Reactivity of Stannane and Silane in the Trifluoromethylation of Pd^{II}: Cyclic Transition State versus Difluorocarbene Release. *Angew. Chem. Int. Ed.* **2018**, *57*, 15081–15085.

49. Fukui, K. The Path of Chemical Reactions – The IRC Approach. *Acc. Chem. Res.* **1981**, *14*, 363–368.

50. Neese, F. The ORCA Program System. *Comput. Mol. Sci.* **2012**, *2*, 73–78.

51. Aziz, H. R.; Singleton, D. A. Concert along the Edge: Dynamics and the Nature of the Border between General and Specific Acid–Base Catalysis. *J. Am. Chem. Soc.* **2017**, *139*, 5965–5972.

52. Ye, L.; Wang, Y.; Aue, G. H.; Zhang, L. Experimental and Computational Evidence for Gold Vinylidenes: Generation from Terminal Alkynes via a Bifurcation Pathway and Facile C-H Insertions. *J. Am. Chem. Soc.* **2012**, *134*, 31–34.

53. Noey, E. L.; Wang, X.; Houk, K. N. Selective Gold(I)-Catalyzed Formation of Tetracyclic Indolines: A Single Transition Structure and Bifurcations Lead to Multiple Products. *J. Org. Chem.* **2011**, *76*, 3477–3483.

54. Zhang, L.; Wang, Y.; Yao, Z-J.; Wang, X.; Yu, Z-X. Kinetic or Dynamic Control on a Bifurcating Potential Energy Surface? An Experimental and DFT Study of Gold-Catalyzed Ring Expansion and Spirocyclization of 2-Propargyl-β-tetrahydrocarbolines. *J. Am. Chem. Soc.* **2015**, *137*, 13290–13300.

55. Mandal, N.; Datta, A. Gold(I)-Catalyzed Intramolecular Diels-Alder Reaction: Evolution of Trappable Intermediates via Asynchronous Transition States *J. Org. Chem.* **2018**, *83*, 11167–11177

56. Li, Y.; Lin, Z. Gold(III)-Catalyzed Intramolecular Cyclization of α-Pyrroles to Pyrrolopyridinones and Pyrroloazepinones: A DFT Study. *Organometallics* 2015, 34, 3538–3545.

57. Paton, R. S.; Maseras, F. Gold(I)-Catalyzed Intermolecular Hydroalkoxylation of Allenes: A DFT study. *Org. Lett.* **2009**, *11*, 2237–2240.

TOC Graphic